An exploration of task based fMRI in neonates using echo-shifting to allow acquisition at longer T_E without loss of temporal efficiency

Giulio Ferrazzi[a,1,*], Rita G. Nunes[a,b,1], Tomoki Arichi[a,c], Andreia O. Gaspar[a,b], Giovanni Barone[a,e], Alessandro Allievi[c], Serge Vasylechko[d], Maryam Abaei[a], Emer Hughes[a], Daniel Rueckert[d], Anthony N. Price[a], Joseph V. Hajnal[a]

[a]*Centre for the Developing Brain, Division of Imaging Sciences & Biomedical Engineering, King's College London, St Thomas' Hospital, Westminster Bridge Rd London SE1 7EH, UK. Telephone: + 44 (0) 20 7188 9145.*
[b]*Instituto de Biofisica e Engenharia Biomedica, Universidade de Lisboa, Faculdade de Ciencias da Universidade de Lisboa, Campo Grande, Lisbon 1749-016, Portugal*
[c]*Department of Biomedical Engineering, Imperial College London, South Kensington Campus London SW7 2AZ, UK*
[d]*Biomedical Image Analysis Group, Department of Computing, Imperial College London, South Kensington Campus London SW7 2AZ, UK*
[e]*Catholic University of Sacred Heart. Largo A. Gemelli 8, Rome 00168, Italy*

Abstract

Optimal Contrast to Noise Ratio of the BOLD signal in neonatal and fetal fMRI has been hard to achieve because of the much longer T_2^* values in developing brain tissue in comparison to those in the mature adult brain. The conventional approach of optimizing fMRI sequences would suggest matching the echo time (T_E) and the T_2^* of the neonatal and fetal brain. However, the use of a long echo time would typically increase the minimum repetition time (T_R) resulting in inefficient sampling.

Here we apply the concept of echo shifting to task based neonatal fMRI in order to achieve an improved Contrast to Noise Ratio and efficient data sampling at the same time. Echo shifted EPI (es-EPI) is a modification of a standard 2D-EPI sequence which enables echo times longer than the time

*Corresponding author
Email address: giulio.ferrazzi@kcl.ac.uk (Giulio Ferrazzi)
[1]Contributed equally to the paper

between consecutive excitations ($T_E > T_S = \frac{T_R}{N_S}$, where N_S is the number of acquired slices and T_S the inter-slice repetition time). The proposed method was tested on neonatal subjects using a passive sensori-motor task paradigm. Dual echo EPI datasets with an identical readout structure to es-EPI were also acquired and used as control data to assess BOLD activation.
From the results of the latter analysis, an average increase of 78 ± 41 % in Contrast to Noise Ratio was observable when comparing late to short echoes. Furthermore, es-EPI allowed the acquisition of data with an identical contrast to the late echo, but more efficiently since a higher number of slices could be acquired in the same amount of time.

Keywords: Neonatal fMRI, Contrast to Noise Ratio, Echo shifting

---

1. Introduction

Most often, the imaging parameters selected for neonatal and fetal fMRI are typical of adult populations rather than optimized for BOLD detection in the developing brain (Fulford and Gowland, 2009; Smyser et al., 2010; Doria et al., 2010; Schöpf et al., 2012; Thomason et al., 2013; Ferrazzi et al., 2014). In order to achieve an optimal Contrast to Noise Ratio (CNR), the sequence echo time T_E should match the average T_2^* across the brain (Bandettini et al., 1994).
Fetal, preterm and neonatal brains are characterized by longer T_2^* values than adults. This is due to their higher content of water and to incomplete myelination, synaptogenesis and synaptic pruning processes (Rivkin et al., 2004).
The difference between these populations is substantial. In healthy adults, T_2^* ranges from 40 to 60 ms at 1.5T (Bandettini et al., 1994). In contrast, for the same field strength, the literature reports T_2^* values of 154 ± 24 ms in the thalamic deep grey matter of healthy fetuses (Vasylechko et al., 2015), and of 137 ± 13 ms for babies born prematurely (Rivkin et al., 2004). T_2^* decreases as a function of age, and in neonates at term equivalent age the same study shows measurements of 127 ± 23 ms.
The relaxation time values quoted above pertain to 1.5T. Figure 1 shows an example T_2^* map for the brain of an infant at term age (41 weeks) scanned during natural sleep. An estimate of T_2^* was calculated from multi echo single shot EPI data acquired on a 3T Philips Achieva system. Data resolution was $2{\cdot}2{\cdot}2.5$ mm^3 and 10 echoes were acquired at echo times $T_E{+}n\Delta T_E = 34{+}n\,57$

ms ($0 \leq n \leq 9$). Details about the fitting procedure are given in the Figure caption. The lower row of the Figure shows a T_2 fast spin echo (FSE) image of the same subject to provide an anatomical reference. This image could not be fully registered onto the EPI data because of geometrical distortions of the latter. All data are presented in the transverse, sagittal and coronal views.

The T_2^* map was windowed within the interval 0 and 280 ms. With such representation, white matter and CSF appear bright and, sometimes, they saturate the scale. In the grey matter, T_2^* is lower, but still considerably high when compared to adult subjects. As an example, three spheres with a diameter of 3 voxels each were placed along the left motor cortex strip and their position is displayed in Figure 1 with coloured circles (T_2^* row, transverse view). Measurements taken on those voxels falling into the spheres led to T_2^* estimates of 102 ± 18 ms, 108 ± 18 ms and 120 ± 32 ms respectively.

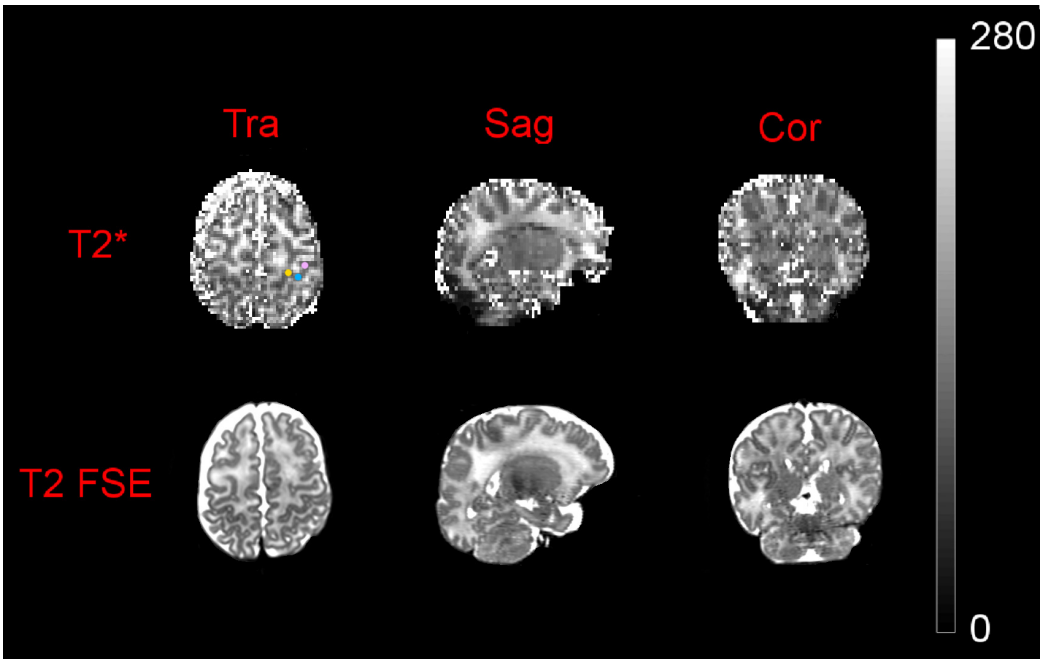

Figure 1: First row: T_2^* map in the infant brain estimated by using the method described in Vasylechko et al. (2015), with a variant to account for local B_0 field variations (Dahnke and Schaeffter, 2005). Second row: FSE anatomical image.

The substantially longer relaxation properties of the infant brain motivate a re-think of 2D-EPI sequences to match the magnetic tissue properties of neonates and fetuses, and raises interesting challenges as longer echo times usually decrease the rate with which data can be acquired. This is also regarded as an important factor in fMRI.
The idea of extending the echo time while maintaining efficient sampling was firstly introduced in Moonen et al. (1992). Since then, echo shifting has found different applications - for example, in the field of T_2^* weighted bolus tracking (Moonen et al., 1994) and diffusion weighted images (DWI) (Delalande et al., 1999). Another popular sequence that implements echo shifting is the PRESTO sequence (Liu et al., 1993).
There have been two other studies whose aim was to perform an es-fMRI experiment (Gibson et al., 2006; Chang et al., 2013). However, while their main focus was to shorten the repetition time allowing, for example, the separation of neuronal signal from cardiac pulsation and respiration (Birn et al., 2006) - our approach is different. Here, for a given and fixed repetition time T_R, we use echo shifting to stretch the echo time T_E allowing closer matching to the magnetic properties of neonatal brain.
To assess whether an increase in BOLD signal sensitivity would be observed, fMRI experiments were performed on neonates with the es-EPI sequence and a conventional 2D-EPI acquisition performed at two different echo times (the longest equivalent to the effective echo time for es-EPI) and a passive motor stimulus was used.
Our aim was to assess whether echo shifting allows access to greater BOLD sensitivity in neonates without loss of temporal efficiency.

2. Materials and Methods

2.1. es-EPI

es-EPI is a modification of a standard 2D-EPI sequence which enables echo times longer than the time between consecutive excitations ($T_E > T_S$).
Figure 2 shows an es-EPI sequence. Similarly to what was presented in Chang et al. (2013), the coloured components indicate the gradients that achieve echo shifting, whereas the black lines represent a normal 2D-EPI sequence. In this representation, dashed lines are part of a standard 2D-EPI readout, but they are not present when performing echo shifting.
The Figure shows two consecutively acquired slices of the entire fMRI acquisition; the signal coming from the j^{th} slice is immediately crushed after

excitation and only gets refocused after excitation of the next slice. The signal coming from the excitation of the $(j+1)^{th}$ slice is then crushed, and later read after the following slice has been excited. Our implementation introduces a phase accumulation of 2π (or multiples) along each pixel in the read, phase encoding and/or slice directions. With this choice, spins positioned symmetrically with respect to the center of every voxel sum up destructively. There is a simple set of constraints that need to be fulfilled in order to achieve echo shifting. These constrains are highlighted in Figure 2, where we indicate with A_x, A_y and A_z the crushers and with B the slice selective gradient. In this example, the phase dispersion along each direction is 2π and the effective echo time is $T_E = T_S + T_E^*$, where T_E^* is the nominal echo time of the corresponding standard EPI sequence.

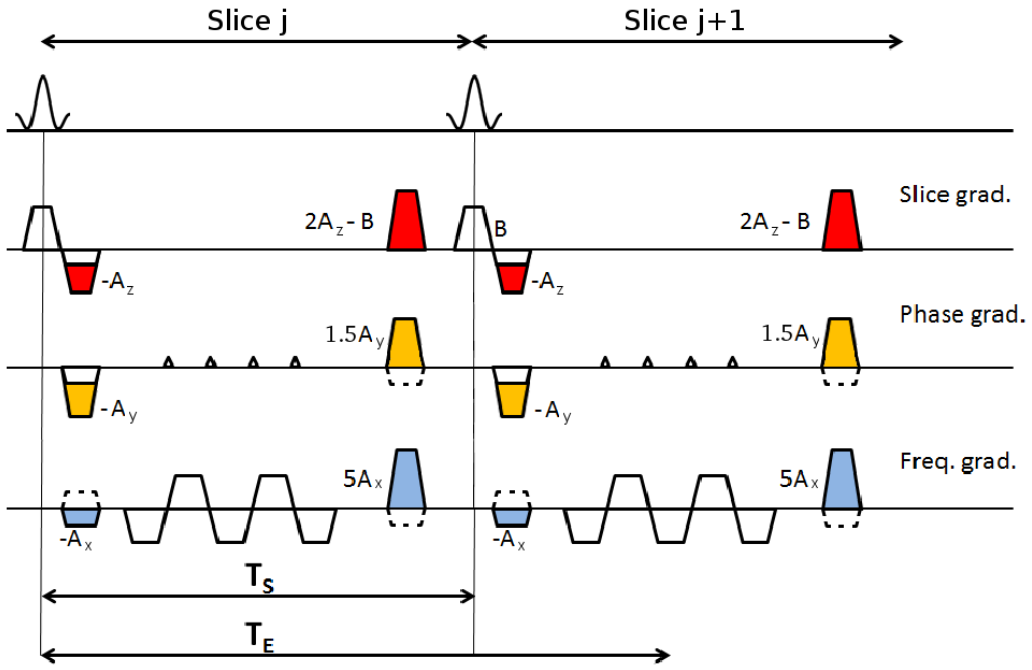

Figure 2: es-EPI sequence. The coloured components highlight the gradients that achieve echo shifting as in Chang et al. (2013), whereas the black lines refer to a standard 2D-EPI sequence. Dashed black lines belong to a standard 2D-EPI sequence and the shift is 2π along each direction.

Let's imagine an experiment in which the signal is shifted *along the read di-*

rection only with an EPI readout that has an even number of phase encode steps.
The green portion of Figure 3 represents the k-space acquisition trajectory achieved with standard EPI. However, a shift is applied along the read and this corresponds to the horizontal direction in the Figure. To achieve this, the polarity of the prephaser gradient of Figure 2 is inverted ($-A_x$ term) and the effect is to move in the opposite direction along k_x (Figure 3, position 1 instead of position 4 as in 2D-EPI). A standard EPI readout is then played out and a shifted k-space plane is acquired (red portion in Figure 3, finishing at position 2). Following this, the refocusing gradient (of area $5A_x$) is applied (Figure 3, position 3) and subsequently the second prephaser gradient belonging to the following excitation (Figure 3, position 4). Only at this stage, the readout encodes the signal coming from the previously excited slice. The same process is then repeated for all other slices.

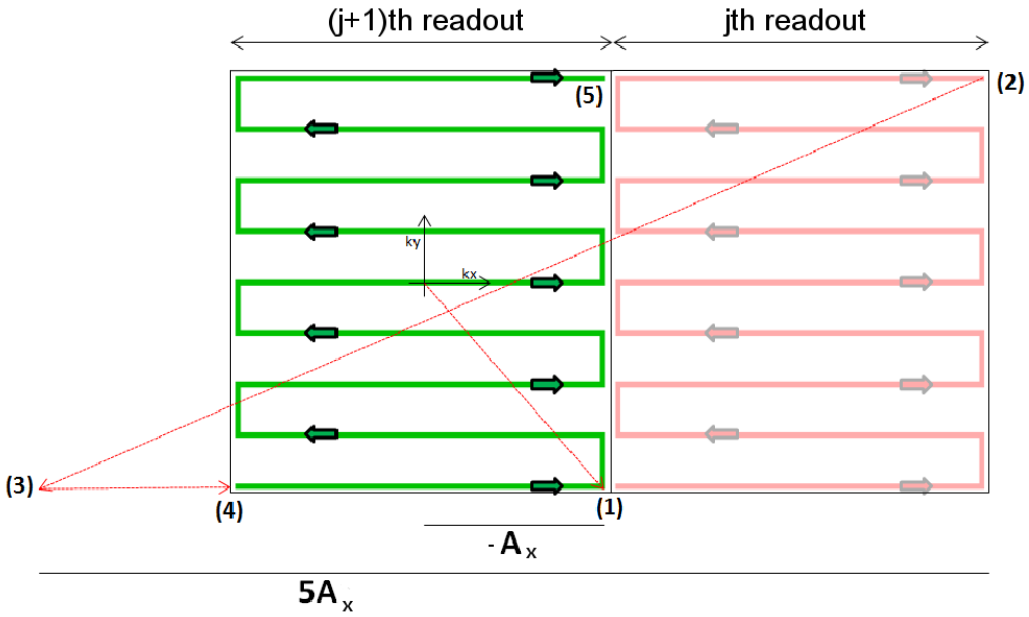

Figure 3: es-EPI k-space trajectory achieved by shifting the signal along the read direction. The phase dispersion is 2π for each voxel.

Equivalent considerations can be derived when considering k_y and k_z.

2.2. Contamination effect and tSNR test

During the $(j+1)^{th}$ readout, there is the potential issue of contamination of the signal corresponding to the j^{th} excitation with that coming from the slice excited by the $(j+1)^{th}$ pulse. If this happens, j^{th} and $(j+1)^{th}$ slices will be encoded together, hindering further analyses. This effect can potentially be very detrimental as the second excitation carries more signal than the first due to the shorter effective T_E^*.

The gradient following the $(j+1)^{th}$ excitation must sufficiently crush the signal excited by that pulse so that it does not contaminate the signal refocused from the j^{th} slice.

To assess this, we characterized the contribution of the signal excited by the $(j+1)^{th}$ pulse onto the $(j+1)^{th}$ readout. When this is null, it should be comparable to noise.

The polarity of the refocusing gradients at the end of each readout was therefore inverted so that the signal coming from the j^{th} slice would not refocus. The strength of the crushers was modified, so that the phase accumulation across each pixel was either 2π or 4π. This was repeated using different combinations of shifts along frequency, phase and slice encoding directions.

All data were acquired on a 3-Tesla Achieva Philips system and the tests were performed on a water phantom. Images were acquired with a T_E^* of 20 ms and a SENSE factor of 2. With this set up, the effective echo time T_E was 63 ms and data resolution $2.5 \cdot 2.5 \cdot 2$ mm^3. A noise reference scan obtained by turning the RF pulse off was also acquired.

We also quantified the temporal Signal to Noise Ratio (tSNR) of the sequence and compared it to an equivalent EPI acquisition. To do so, another bottle phantom was scanned at an isotropic resolution of 2 mm, repetition time T_R of 2545 ms and effective T_E of 75 ms with a SENSE factor of 2.

To match the repetition time of the standard EPI sequence to echo shifting, roughly half of the slices were acquired. Resolution and echo time were kept the same and, in total, 200 volumes were imaged. Image based shimming was employed (Schneider and Glover, 1991), and shim values kept constant across the 2 scans. Finally, due to the different coverage achieved in the two acquisitions, the tSNR was evaluated only within overlapping regions.

Standard reconstruction could not be used on the scanner. By using echo-shifting, the slice position corresponding to each readout no longer matches the slice excited by the most recent RF pulse. This would cause SENSE reconstruction to fail unless the labelling of the slices is corrected. To avoid this problem, all reconstructions were performed offline with the ReconFrame

sofware (`http://www.gyrotools.com/products/gt-recon.html`), which allows the rearrangement of the acquired data and to pair it with the correct sensitivities.

2.3. Neonatal fMRI experiments

This section focuses on the use of echo shifting to perform an optimized neonatal fMRI experiment. The acquisitions were performed on a 3T system (same scanner as before) using a standard 32 channel head coil. Ethical approval for the study was attained from the NHS research ethics committee, and written parental consent was obtained prior to all sessions of data acquisition. The study population consisted of 5 healthy infants at term (3 of which were sedated with oral chloral hydrate at 30-50 mg/kg/dose prior to scanning) of 41.4 $\pm$ 1.14 weeks at scan; and 8 preterm infants of 33.6 $\pm$ 1.5 weeks at scan (images acquired during natural sleep). One preterm infant was known to have intra-uterine growth retardation (IUGR). Infants with focal brain pathology (such as stroke or intracerebral hemorrhage), diagnosed metabolic or genetic abnormalities, and those with a history of requiring vigorous resuscitation at delivery were excluded from the study.

es-EPI data were acquired with T_E and T_R of 75 and 2545 ms respectively. In plane resolution was 2 mm, and the SENSE factor 2. Other acquisition parameters were: field of view; $160 \cdot 136 \cdot 92$ mm^3, Data matrix size; $80 \cdot 68$, Water fat shift separation; 12.9 pixels.

To test the hypothesis that echo shifting provides an improved sensitivity to BOLD contrast functional responses, dual-echo single shot EPI datasets were also acquired with T_E of 25 and 75 ms, an identical T_R of 2545 ms and matched spatial resolution and bandwidth. To ensure identical sampling properties, a reduced number of slices was again used in the dual-echo experiments (20) compared to the es-EPI sequences(46). The slice thickness was either 2 or 3 mm (the latter selected when better coverage of the motor cortex was required for the dual echo acquisitions) and all images were acquired in the axial plane. The number of frames was 125 (total scan time roughly 5 minutes and 20 seconds) and echo shifting was the first scan to be run.

A sensori-motor stimulus was achieved by using a fully automated and pneumatically driven fMRI compatible robotic interface designed and built for use with fragile neonatal subjects (Allievi et al., 2013). The interface was placed onto the right wrist and hand of the majority of infants prior to scanning

(the left hand was used for the IUGR infant due to pre-existing venous access on the right hand).
Precisely controlled and highly reproducible passive extension/flexion movements of the wrist were achieved through a piston actuator, controlled by compressed air and dedicated software (Allievi et al., 2013). The timing of stimulation was synchronized to the image acquisition via detection of the MRI scanner TTL pulse emitted with each T_R. A simple block experimental paradigm was used, consisting of alternating 22.9 second periods (9 T_R) of 0.5 Hz wrist extension/flexion ('on') and rest ('off').
Data were analysed with tools implemented in the FMRIB software library (FSL; `http://fsl.fmrib.ox.ac.uk/fsl/fslwiki/` (Smith et al., 2004)). Standard pre-processing steps were applied to the data after visual identification of high motion frames; these included linear spatial realignment to the middle volume, spatial smoothing (Gaussian filter of 4 mm FWHM), slice timing correction, and high-pass filtering (cut-off 50 seconds). Data were then analysed using the General Linear Model (GLM) as implemented in FEAT, with the input boxcar function convolved with a set of linear basis functions optimised for use with neonatal subjects (Arichi et al., 2012).
CNR and the % of BOLD signal change were then quantified in all datasets. CNR is defined as the ratio between the variation of the BOLD signal ΔB and the standard deviation of the noise time series. A more practical formula for its evaluation is however given in Krüger et al. (2001) and Wald (2012), where

$$CNR = tSNR \cdot T_E \cdot \Delta R_2^* \tag{1}$$

In here, ΔR_2^* represents the change in $R_2^* = \frac{1}{T_2^*}$ that accompanies activation. In this study ΔR_2^* is not known, but it is dependent on the brain activation rather than acquisition parameters, so was treated as a constant in all single subject comparisons between acquisitions.
Before calculating % of BOLD signal change, all time series were low pass-filtered with a standard Butterworth filter (cut-off frequency 0.12 Hz) to remove high frequency noise.
We finally compare the z statistics from all activation maps in the 3 sequences.

3. Results

3.1. Contamination effects and tSNR test

Figure 4 shows the results obtained from the contamination experiment. The first row shows a reference scan acquired by using the standard 2D-EPI sequence. The noise scan is presented in the second row. Noise has a structured appearance because of SENSE (Pruessmann et al., 1999). Nevertheless, this is the image that we would like to reproduce when using echo shifting with the refocusing gradients acting as crushers instead.

Rows A-G show echo shifted images for different directions and degrees of gradient spoiling.

In our experiments, shifting only along one direction did not completely suppress the signal. This effect becomes less prominent using stronger gradients (second column). Case A: imposing a crusher along the read direction direction (horizontal in the Figure) produced an edge artefact along the phase encoding direction (vertical); echo shifting can in fact be seen as a shift of the sampled k-space domain as presented in Figure 3. When a shift is applied along the read direction, the effect is that the k-space region actually sampled is shifted to the right or to the left along the k_x direction relative to a standard EPI readout. However, the same range of k_y spatial frequencies is still sampled as in the corresponding 2D-EPI sequence. After Fourier transforming, the result is an edge artefact along the phase encoding direction. Similar considerations can be done when imposing the shift along the phase encoding direction (case B). Also, when the shift is applied along the read and phase at the same time (case D), the edge artefact appeared rotated by 45° along the xy plane.

Imposing a 2π shift along the slice direction (case C) did not suppress the signal entirely. However, the effect was reduced when applying a shift of 4π. Combining slice with read or phase shifts (cases E and F) suppressed the signal well. There were however remaining localized components of signal.

When shifting along all three directions at the same time (case G), the signal was well suppressed both using a shift of 2π and 4π and the latter was used for the subsequent in vivo acquisitions.

Finally, the tSNR test showed almost identical values for echo shifting and standard EPI run at long echo times (18.5 ± 4.4 and 18.7 ± 4.3 in the first and second case), suggesting that the stability of the signal is not compromised.

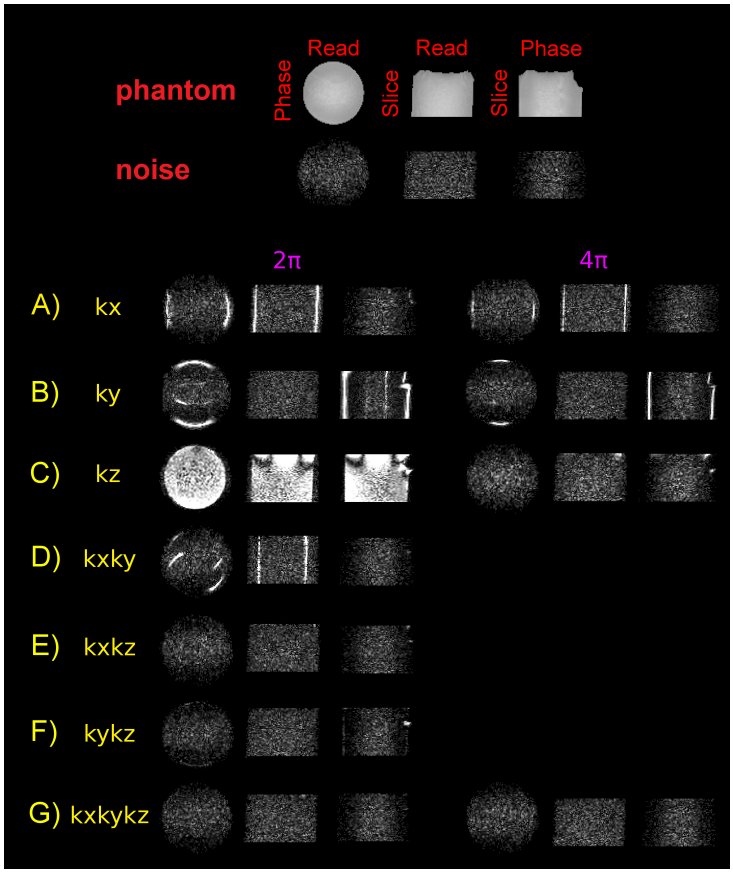

Figure 4: Echo shifted contamination experiment: first row shows the reference scan and the second the noise measurement. Read, phase and slice directions are outlined in red. Rows A to G show the contaminating signal excited by the $(j+1)^{th}$ RF pulse for different combinations of shifts along read (k_x), phase (k_y) and slice (k_z) directions. First and second columns correspond to shifts of 2π and 4π. When a specific combination of shifts/strengths is not present, that set of data was not acquired. Apart from the top row image, all images have identical display settings.

3.2. Echo Shifting on neonatal data with task fMRI

In total, the scanning duration for each scan was 5 minutes and 20 seconds. There was therefore a high chance for a neonate to move during this period. Motion corrupted frames were removed from all datasets. When both dual

and echo shifted EPI could be analysed, the same number of frames was always removed from both time series so as not to favour either of the two acquisitions when assessing BOLD activation. Table 1 reports the success rate of this study plus the age at scan of all infants (ascending order). When 'Yes', activation resembling the predicted behaviour was found in the left hemisphere in the motor cortex (right motor cortex for the baby with IUGR). In unsuccessful datasets ('No'), head motion was either too great or frequent to allow accurate analysis even following frame removal and standard motion correction steps during data pre-processing.
In total, there were two cases in which both the es-EPI and dual echo data did not show activation in the motor cortex. These cases were removed from this study and they are not reported in Table 1.

Baby	Weeks	Dual-Echo	es-EPI	Retained frames
1	32	No	Yes	125
2	32	Yes	Yes	105
3	33	Yes	Yes	125
4	33	Yes	No	125
5	33	Yes	No	125
6	35	Yes	No	125
7	35	Yes	Yes	99
8	41	Yes	No	78
9	41	No	Yes	90
10	42	Yes	Yes	70
11	43	Yes	Yes	74

Table 1: Age of scan (ascending order) in weeks and positive/negative outcome (Yes/No) for dual-echo and es-EPI. The number of retained frames is on the right hand side.

Figure 5 presents transverse, coronal and sagittal views of the es-EPI data (first row) and of the dual-echo data (second and third rows) for subject number 3. Tissue contrast is very different between the echoes of the dual echo sequence, which also provided only partial brain coverage given the same repetition time used in all acquisitions. Overlaid on the EPI images, are the clusters of activated voxels obtained by the GLM analysis. Activated clusters are in the left contralateral primary somatosensory cortex.
Figure 6 (A) reports the % of BOLD signal averaged over the the top quartile of active cluster for those subjects in which there was a detectable activation

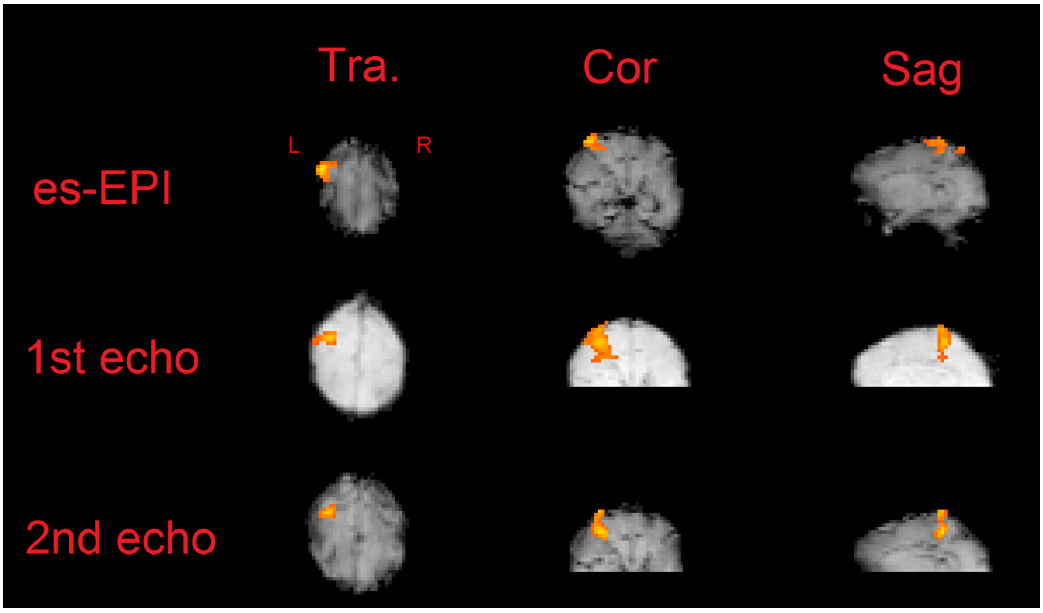

Figure 5: Left: transverse, coronal and sagittal views of the activated clusters for es-EPI data (first row) and dual-echo experiments (second and third rows) for subject number 3.

in one or both acquisitions. Left plots show BOLD activation in dual echo data, and on the right the same for es-EPI.
The data relative to the second echo tends to vary more than the first in all cases.
In total, there were 5 cases in which both echo shifting and dual echo EPI produced clear activation signals in the motor area.
Table 2 shows the standard deviation of BOLD signal change in % for all subjects. In all the dual echo experiments that were successful, there was a larger BOLD activation during the second echo. We also observed a similar trend in echo shifted data - and means and standard deviations of the % of BOLD signal change across all subjects were $0.3 \pm 0.1\%$ and $0.7 \pm 0.3\%$ in the dual echo sequence, and $1 \pm 0.5\%$ for es-EPI.
Figure 6 (B) reports the CNR within the active clusters for all subjects. The latter was estimated by using equation 1.
Apart from subject number 8, there is a substantial increase in the second echo of all dual echo datasets, with the CNR being roughly the double than

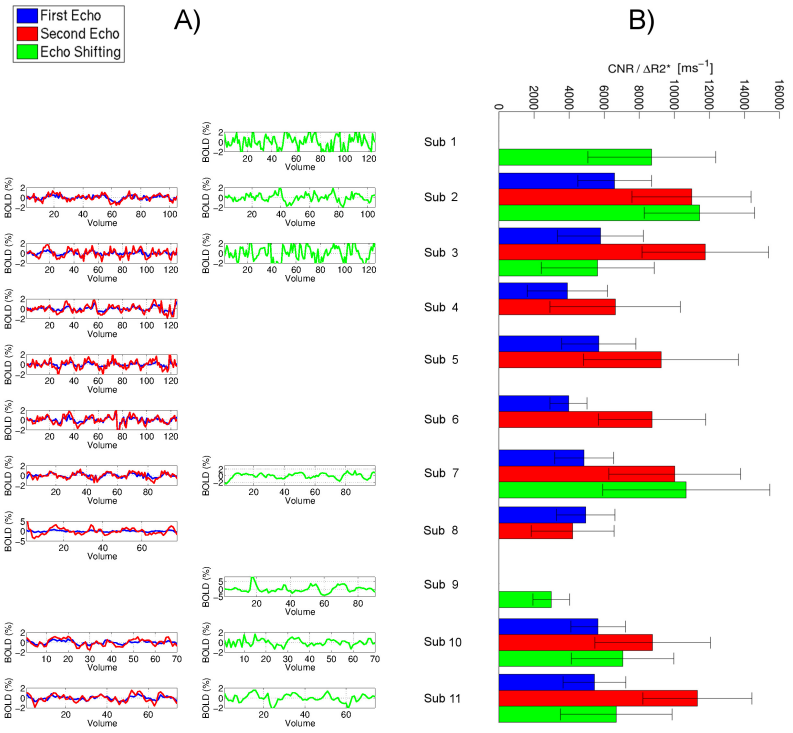

Figure 6: A) Left column: BOLD signal change over active clusters in the motor cortex converted in % signal change for each subject (rows). Blue plots correspond to the data acquired with an echo time of 25 ms, red 75 ms. Right column: BOLD signal change achieved with echo shifting. Plots that are not present correspond to data where there was either no activation or too much motion. B) Contrast to Noise Ratio of the BOLD signal (scaled by ΔR_2^*) in each subject. Data ordering follows Table 1.

in the first echo. This increase approximately follows the theoretical predictions - by hypothesising a basal T_2^* value of 102 ms (taken as the lowest T_2^* value measured during the test reported in Figure 1), we get that the ratio $\frac{CNR_{75}}{CNR_{25}} = \frac{tSNR_{75}T_{E,75}\Delta R_2^*}{tSNR_{25}T_{E,25}\Delta R_2^*} = \frac{e^{-\frac{75}{102}}}{e^{-\frac{25}{102}}} \cdot \frac{75}{25} = 1.84$. Here, the tSNR is modelled as $\frac{S \cdot e^{-\frac{T_E}{T_2^*}}}{\sigma}$, where S is the available signal immediately after excitation and σ the standard deviation of the noise time series. S and σ are also assumed to be the same for both echoes.

Baby	First Echo	Second Echo	Echo Shifted
1	–	–	1.03 %
2	0.34 %	0.52 %	0.63 %
3	0.25 %	0.64 %	1.19 %
4	0.35 %	0.66 %	–
5	0.27 %	0.66 %	–
6	0.42 %	0.68 %	–
7	0.35 %	0.5 %	0.79 %
8	0.28 %	1.47 %	–
9	–	–	1.94 %
10	0.34 %	0.70 %	0.65 %
11	0.34 %	0.59 %	0.67 %

Table 2: Standard deviation of the BOLD signal in % for the 3 sequences in each subject. The symbol '-' indicates datasets with no detected activation.

Data from the second echo of the multi-echo and echo-shifted acquisitions are also in partial agreement. The discrepancy, when present, can be explained by motion.

Figure 7 reports the CNR plotted against the standard deviation of the absolute displacement traces obtained from the GLM. Blue, red and green points correspond to dual echo and echo shifted datasets. A clear feature of the data is a significant linear trend in $\frac{CNR}{\Delta R_2^*}$ with the simple marker of the magnitude of the motion (R^2 of 0.54, 0.22 and 0.79 in each case).

Figure 8 shows the CNR of Figure 6 (B) with the effect of motion factorized out. This was achieved by multiplying the data points of Figure 7 by the factor $\frac{b}{a \cdot x_{mot} + b}$, where a and b are the coefficients from the linear fit, and x_{mot} the variable in the horizontal axis in Figure 7.

The CNR of echo shifted and second echo acquisitions are now in agreement. Furthermore, when comparing long to short echoes, an average increase of 78 $\pm$ 41 % in CNR was observed across all subjects. However, we still note some discrepancies for subject number 11, where even after factorizing motion out, there is a considerable difference between echo shifting and the second echo of the double echo acquisition. It is however hard to say what might have caused this; a possible explanation could be that - since the fit of the model to the data was performed on each dataset independently - active regions might have been subjected to slightly different ΔR_2^* values. Furthermore,

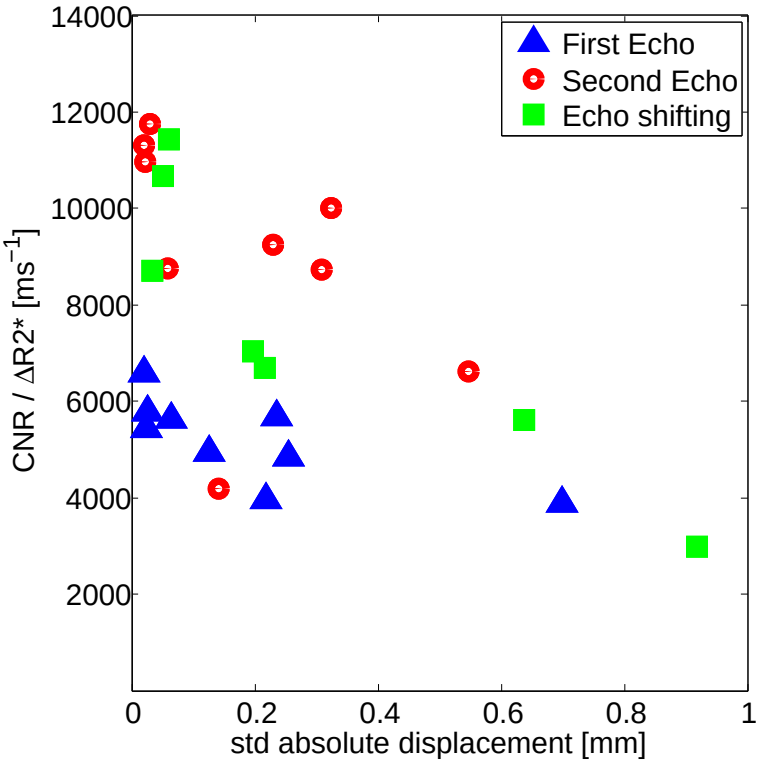

Figure 7: Contrast to Noise Ratio (scaled by ΔR_2^*) plotted against the standard deviation of the translational displacements for each subject as determined from the motion correction used in the fMRI analysis. Blue, red and green points correspond to dual echo and echo shifted datasets.

the process of factorizing motion out can be subjected to bias. This may derive from the metric that was chosen to represent the extent of motion. We finally compared the z statistics from the GLM analysis. In this study, we do not observe significant differences between the z scores of first/second echoes and echo shifting (mean across all subjects 3.12 $\pm$ 0.35, 3.04 $\pm$ 0.21 and 3.03 $\pm$ 0.1).

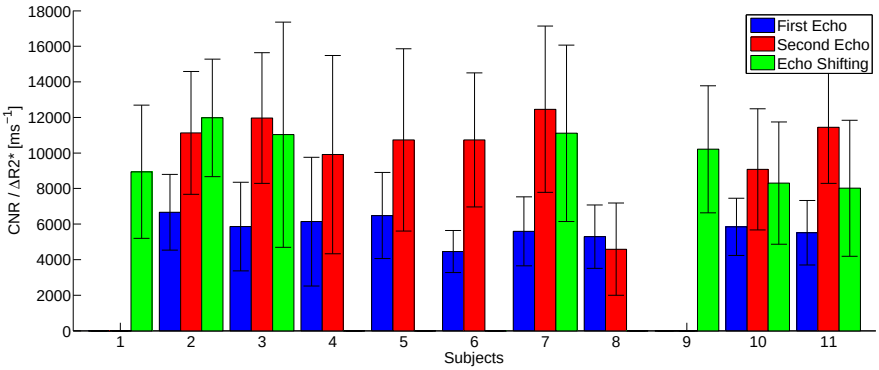

Figure 8: Contrast to Noise Ratio of Figure 6 (B) with the effect of motion factorized out.

4. Discussion and Conclusions

The purpose of this study is to gather evidence as to the efficacy and suitability of echo shifting as a means to achieve time efficient fMRI acquisitions that can be tuned to match the longer T_2^* of neonatal brain as compared to adult brain. Conventional EPI sequences typically commence the readout immediately after the excitation process is complete, and in fact there is often a trade off between resolution and minimal echo time. Increasing the duration of the readout reduces the imaging bandwidth in the phase encode direction which can cause problems with excessive spatial distortion. Deliberately increasing the echo time of EPI sequences to increase BOLD sensitivity when T_2^* is long can be achieved by introducing a delay between excitation and the start of the readout. This reduces efficiency by forcing T_R to increase.
The echo shifting approach tested in this work allows the T_R and hence the temporal sampling rate to remain almost unchanged when T_E is increased, so that sequence efficiency can be preserved. The study has focused on demonstrating that the echo shifting concept can be implemented as part of a task based paradigm for neonates without loss of performance. This resulted in a study designed to compare echo-shifted data with matched dual echo data that otherwise has the same timings.
It is beyond the scope of this study to infer on the echo time to be used in fetal and neonatal fMRI studies. However, after the selection of the optimal T_E, the echo shifting sequence can be further optimized to be as efficient

as possible. Furthermore, having established that echo shifting is a viable approach, there is the option to lengthen T_E by skipping more than one T_R period, so that it becomes possible to optimize both T_E for sensitivity and T_R for efficiency. We think this is an exciting prospect which would require tuning depending on the specific brain region being studied.

The equivalence between the properties of es-EPI and the second echo of the of dual echo EPI signal was first assessed using a phantom. The result from that test suggested that a shift of the signal along the three orthogonal directions x, y and z is the safest to achieve good suppression of the primary echo. Other studies (for example, Gibson et al. (2006)) have employed the spoilers only along one direction. Precise results depend on the magnitude of the spoilers used to crush the signal and it is likely that equivalent performance can be achieved with different spoiler combinations provided the spoiler magnitude is chosen appropriately.

Regarding the in vivo data, the choice of performing a task based fMRI experiment as opposed to gathering resting state data enabled the identification of a specific signal change following stimulation which could be quantified and therefore compared between the different sequences. Having a model able to predict the BOLD response proved to be important when trying to separate useful signal from other sources. However, the advantages offered by echo shifting in neonatal fMRI should remain the same with resting state data.

The task activation experiments were extremely challenging, particularly as there was a need to perform two task activation runs, which increased the chance that the baby could wake up or cry during acquisition. When that happened, we always halt the examination as the baby's safety and comfort are obviously the first priorities.

Motion is a common problem in neonatal fMRI. In this study, motion corrupted frames were removed from the fMRI time series. Head motion is known to be a significant source of bias and inaccuracy in fMRI data analysis, and when not appropriately accounted for can lead to false positive results and artificial patterns of correlation (Power et al., 2012). As the aim was to assess CNR, we could not reliably trust segments of data with motion. However, discarding data decreases statistical activation power. Furthermore, several other factors may have contributed to the detectability of activation signal in some of the experiments. These include technical difficulties or habituation effects (Poellinger et al., 2001). In this study, the scanning order of echo shifting and dual echo EPI was fixed. It remains to be assessed whether a randomized approach would have been more beneficial in terms of BOLD

signal detection.
Nonetheless, 5 examples (subjects 2, 3, 7, 10 and 11 of Table 1) were obtained consistent with the proposition that echo shifting does allow access to longer echo times without loss of temporal efficiency. Furthermore, when successful, the data acquired at longer echo times generally provided fMRI data with increased CNR. Despite an increase in CNR, the z scores did not change. This suggests that the selection of the optimal echo time T_E should also take into consideration other factors such as the decrease in tSNR that happen at long echo times. Despite the T_2 being longer in immature brains, the issue of signal dropout at air-tissue interfaces at longer T_E remains. In this sense, the selection of a motor task experiment should not constitute an issue, since the field is usually homogeneous over these regions.
To conclude, this preliminary data suggests that echo shifting is a viable approach that allows BOLD sensitivity to be increased when T_2^* is longer without sacrificing scan efficiency or temporal sampling rates. The methodology could be particularly suitable for fetal fMRI studies, where signal dropout is less significant as air/tissue boundaries are generally absent in the womb (Ferrazzi et al., 2014). The sequence would also need to be integrated with fat suppression of the maternal tissue, which is a simple addition to what has been demonstrated here. Echo shifting is completely compatible with multiband methods (Larkman et al., 2001; Feinberg and Setsompop, 2013; Boyacioglu et al., 2015), and this combination could potentially provide higher sampling rates at long echo times.

Author's contributions.
GF and RN made equal contributions to the work, and were involved in all aspects including: experimental design, data collection, data analysis and interpretation as well as manuscript preparation.

Acknowledgements.

GF thanks the Wellcome-EPSRC Medical Engineering Centre for a studentship. This research was supported by the MRC through a strategic research Grant (MR/K006355/1) and the EPSRC through programme grant EP/H046410/1.
Support for this work was also provided by the Medical Research Council, Engineering and Physical Sciences Research Council, National Institute for Health Research Comprehensive Biomedical Research Centre awards to Guys

and St Thomasł' National Health Service Foundation Trust in partnership with Kings College London and Kings College Hospital NHS Foundation Trust, and the Garfield Weston Foundation.

RN acknowledges funding from the Portuguese Foundation for Science and Technology, under the FCT Investigator Programme (IF/00364/2013).

Allievi, A., Melendez-Calderon, A., Arichi, T., Edwards, A., Burdet, E., 2013. An fMRI compatible wrist robotic interface to study brain development in neonates. Annals of biomedical engineering 41 (6), 1181–1192.

Arichi, T., Fagiolo, G., Varela, M., Melendez-Calderon, A., Allievi, A., Merchant, N., Tusor, N., Counsell, S. J., Burdet, E., Beckmann, C. F., et al., 2012. Development of BOLD signal hemodynamic responses in the human brain. Neuroimage 63 (2), 663–673.

Bandettini, P. A., Wong, E. C., Jesmanowicz, A., Hinks, R. S., Hyde, J. S., 1994. Spin-echo and gradient-echo EPI of human brain activation using BOLD contrast: a comparative study at 1.5 T. NMR in Biomedicine 7 (1-2), 12–20.

Birn, R. M., Diamond, J. B., Smith, M. A., Bandettini, P. A., 2006. Separating respiratory-variation-related fluctuations from neuronal-activity-related fluctuations in fMRI. Neuroimage 31 (4), 1536–1548.

Boyacioglu, R., Schulz, J., Norris, D., 2015. Multiband echo shifted epi. In: Proc ISMRM MultiBand workshop.

Chang, W.-T., Nummenmaa, A., Witzel, T., Ahveninen, J., Huang, S., Tsai, K. W.-K., Chu, Y.-H., Polimeni, J. R., Belliveau, J. W., Lin, F.-H., 2013. Whole-head rapid fMRI acquisition using echo-shifted magnetic resonance inverse imaging. Neuroimage 78, 325–338.

Dahnke, H., Schaeffter, T., 2005. Limits of detection of SPIO at 3.0 T using T2* relaxometry. Magnetic resonance in medicine 53 (5), 1202–1206.

Delalande, C., de Zwart, J. A., Trillaud, H., Grenier, N., Moonen, C. T., 1999. An echo-shifted gradient-echo MRI method for efficient diffusion weighting. Magnetic resonance in medicine 41 (5), 1000–1008.

Doria, V., Beckmann, C. F., Arichi, T., Merchant, N., Groppo, M., Turkheimer, F. E., Counsell, S. J., Murgasova, M., Aljabar, P., Nunes, R. G., et al., 2010. Emergence of resting state networks in the preterm human brain. Proceedings of the National Academy of Sciences 107 (46), 20015–20020.

Feinberg, D. A., Setsompop, K., 2013. Ultra-fast MRI of the human brain with simultaneous multi-slice imaging. Journal of Magnetic Resonance 229 (0), 90–100.

Ferrazzi, G., Murgasova, M. K., Arichi, T., Malamateniou, C., Fox, M. J., Makropoulos, A., Allsop, J., Rutherford, M., Malik, S., Aljabar, P., et al., 2014. Resting state fMRI in the moving fetus: A robust framework for motion, bias field and spin history correction. NeuroImage 101 (1), 555–568.

Fulford, J., Gowland, P. A., 2009. The emerging role of functional MRI for evaluating fetal brain activity. In: Seminars in perinatology. Vol. 33. Elsevier, pp. 281–288.

Gibson, A., Peters, A. M., Bowtell, R., 2006. Echo-shifted multislice EPI for high-speed fMRI. Magnetic resonance imaging 24 (4), 433–442.

Krüger, G., Kastrup, A., Glover, G. H., 2001. Neuroimaging at 1.5 T and 3.0 T: comparison of oxygenation-sensitive magnetic resonance imaging. Magnetic resonance in medicine 45 (4), 595–604.

Larkman, D. J., Hajnal, J. V., Herlihy, A. H., Coutts, G. A., Young, I. R., Ehnholm, G., 2001. Use of multicoil arrays for separation of signal from multiple slices simultaneously excited. Journal of Magnetic Resonance Imaging 13 (2), 313–317.

Liu, G., Sobering, G., Duyn, J., Moonen, C. T., 1993. A. functional mri technique combining principles of echo-shifting with a train of observations (PRESTO). Magnetic resonance in medicine 30 (6), 764–768.

Moonen, C. T., Barrios, F. A., Zigun, J. R., Gillen, J., Liu, G., Sobering, G., Sexton, R., Woo, J., Frank, J., Weinberger, D. R., 1994. Functional brain MR imaging based on bolus tracking with a fast T 2-sensitized gradient-echo method. Magnetic resonance imaging 12 (3), 379–385.

Moonen, C. T., Liu, G., Gelderen, P. V., Sobering, G., 1992. A fast gradient-recalled MRI technique with increased sensitivity to dynamic susceptibility effects. Magnetic resonance in medicine 26 (1), 184–189.

Poellinger, A., Thomas, R., Lio, P., Lee, A., Makris, N., Rosen, B. R., Kwong, K. K., 2001. Activation and habituation in olfactionan fMRI study. Neuroimage 13 (4), 547–560.

Power, J. D., Barnes, K. A., Snyder, A. Z., Schlaggar, B. L., Petersen, S. E., 2012. Spurious but systematic correlations in functional connectivity MRI networks arise from subject motion. Neuroimage 59 (3), 2142–2154.

Pruessmann, K. P., Weiger, M., Scheidegger, M. B., Boesiger, P., et al., 1999. SENSE: sensitivity encoding for fast MRI. Magnetic resonance in medicine 42 (5), 952–962.

Rivkin, M., Wolraich, D., Als, H., McAnulty, G., Butler, S., Conneman, N., Fischer, C., Vajapeyam, S., Robertson, R., Mulkern, R., 2004. Prolonged t*2 values in newborn versus adult brain: implications for fMRI studies of newborns. Magnetic resonance in medicine 51 (6), 1287–1291.

Schneider, E., Glover, G., 1991. Rapid in vivo proton shimming. Magnetic Resonance in Medicine 18 (2), 335–347.

Schöpf, V., Kasprian, G., Brugger, P., Prayer, D., 2012. Watching the fetal brain at "rest". International Journal of Developmental Neuroscience 30 (1), 11–17.

Smith, S. M., Jenkinson, M., Woolrich, M. W., Beckmann, C. F., Behrens, T. E., Johansen-Berg, H., Bannister, P. R., De Luca, M., Drobnjak, I., Flitney, D. E., et al., 2004. Advances in functional and structural MR image analysis and implementation as FSL. Neuroimage 23, S208–S219.

Smyser, C. D., Inder, T. E., Shimony, J. S., Hill, J. E., Degnan, A. J., Snyder, A. Z., Neil, J. J., 2010. Longitudinal analysis of neural network development in preterm infants. Cerebral Cortex 20 (12), 2852–2862.

Thomason, M. E., Dassanayake, M. T., Shen, S., Katkuri, Y., Alexis, M., Anderson, A. L., Yeo, L., Mody, S., Hernandez-Andrade, E., Hassan, S. S., et al., 2013. Cross-hemispheric functional connectivity in the human fetal brain. Science translational medicine 5 (173), 1–10.

Vasylechko, S., Malamateniou, C., Nunes, R. G., Fox, M., Allsop, J., Rutherford, M., Rueckert, D., Hajnal, J. V., 2015. T2* relaxometry of fetal

brain at 1.5 Tesla using a motion tolerant method. Magnetic Resonance in Medicine 73 (5), 1795–1802.

Wald, L. L., 2012. The future of acquisition speed, coverage, sensitivity, and resolution. NeuroImage 62 (2), 1221–1229.

Williams, L.-A., Gelman, N., Picot, P. A., Lee, D. S., Ewing, J. R., Han, V. K., Thompson, R. T., 2005. Neonatal brain: Regional variability of in vivo MR imaging relaxation rates at 3.0 T - initial experience. Radiology 235 (2), 595–603.